Presentation of electromagnetic multichannel data: The signal space separation method

Samu Taulu[a] and Matti Kajola
Elekta Neuromag Oy, Helsinki 00510, Finland

(Received 6 August 2004; accepted 22 April 2005; published online 21 June 2005)

Measurement of external magnetic fields provides information on electric current distribution inside an object. For example, in magnetoencephalography modern measurement devices sample the magnetic field produced by the brain in several hundred distinct locations around the head. The signal space separation (SSS) method creates a fundamental linear basis for all measurable multichannel signal vectors of magnetic origin. The SSS basis is based on the fact that the magnetic field can be expressed as a combination of two separate and rapidly converging expansions of harmonic functions with one expansion for signals arising from inside of the measurement volume of the sensor array and another for signals arising from outside of this volume. The separation is based on the different convergence volumes of the two expansions and on the fact that the sensors are located in a source current-free volume between the interesting and interfering sources. Individual terms of the expansions are shown to contain uncorrelated information of the underlying source distribution. SSS provides a stable decomposition of the measurement into a fundamental device-independent form when used with an accurately calibrated multichannel device. The external interference signals are elegantly suppressed by leaving the interference components out from the reconstruction based on the decomposition. Representation of multichannel data with the SSS basis is shown to provide a large variety of applications for improved analysis of multichannel data. [DOI: 10.1063/1.1935742]

I. INTRODUCTION

Measurement of magnetic fields has established an invaluable role in studies of electromagnetic phenomena. Today, superconducting quantum interference device (SQUID) sensors provide generally the best sensitivity in recordings of very small magnetic fields, such as the biomagnetic signals associated with normal and pathological functions of excitable cells in the human body ($\sim 10^{-10}$–10^{-14} T).[1] SQUID sensors are typically operated in liquid helium (4 K),[2] but also high-temperature superconductors (180 K) have been applied in some biomagnetic studies.[2] Recent development of other sensor technologies, such as magnetoresistive elements[3] and optical magnetometers,[4] has improved the sensitivity and opened exciting possibilities for detection of very weak magnetic fields.

In many applications the magnetic field is detected with one or few magnetic sensors. However, there are applications, such as studies of the sources of biomagnetic signals outside of the head [magnetoencephalography (MEG)] or the thorax [magnetocardiography (MCG)], where simultaneous recordings at multiple sites are necessary.[5] The number of SQUID sensors in commercially available magnetometers covering the whole head is over 250. In principle, also other sensor types referred to above could be applied in the multichannel biomagnetic studies.

In MEG and MCG, the electric current distributions in the body are examined by measuring the magnetic field outside of the subject. These studies are usually done by multichannel measurement devices comprising spatially distinct sensors designed to obtain representative measurements of the biomagnetic field. The finest geometric details of the magnetic field, however, decay rapidly as a function of distance from the source and only relatively coarse features exceed the noise level of the sensors located farther than 2–4 cm from the skin. Consequently, the number of degrees of freedom of measurable MEG signals is less than 200,[6,7] but increasing the number of sensors beyond that provides oversampling and statistically reliable data. The high number of channels of the modern measurement devices encourages to compress the measured data into basic components which contain all information derivable from a measurement and are suitable for various signal processing and data analysis tasks.

The multichannel measurements are discretizations of the field and can be presented as signal vectors comprising the measured values of all channels. Therefore, it is natural to discretize also the magnetic field by a truncated basis function expansion with terms sorted by increasing content of fine detail. By starting from the coarse features of the field and advancing towards finer details with increasing order of expansion, we can explain any measurable signal of magnetic origin with a fewer number of basis functions than channels of modern multichannel devices. In this way, a fundamental linear model with suitable basis vectors spans all measurable signals of magnetic origin. Consequently, any measured signal vector can be uniquely decomposed into device-independent components corresponding to these basis vectors.

In this paper we present the signal space separation

[a]Electronic mail: samu.taulu@neuromag.fi

(SSS) method which restricts the measured signals into a signal subspace spanning all measurable signals obeying Maxwell's equations. We formulate the SSS basis for the quasistatic approximation which allows to express the magnetic field as the gradient of a harmonic scalar potential. We also show that the magnetic field can be expressed as a combination of two separate expansions, with one expansion for signals arising from inside of the measurement volume of the sensor array and another one for signals arising outside of this volume. The separation is based on the different convergence volumes of the two expansions and on the fact that the sensors are located in a current-free volume between the interesting and interfering sources.

In the case of vector spherical harmonics, individual terms of the expansions are shown to contain uncorrelated information of the underlying source distribution.

SSS improves and facilitates signal processing and analysis of multichannel MEG data dramatically. The method elegantly solves the basic problem of biomagnetic measurements: suppression of the external interference without distorting the inherently weak MEG signals. Furthermore, it provides, e.g., a simple and robust method to compensate for signal distortions caused by movement of the subject possibly having magnetic impurities attached on the head and the body, to measure physiological dc, and to calibrate the sensors with a very high accuracy. The basic vector components decomposed from the measured signals can be used for simpler and more efficient source modeling than the raw measurement values of the channels. We show this by expressing the components in the lead field form comparable to the lead field form of the channels presented in Refs. 5, 8, and 9.

The purpose of this paper is to present the theoretical foundation of the SSS method. Comprehensive practical demonstrations showing the success of SSS are presented in another publication.[10]

II. BASIC PROBLEMS IN BIOMAGNETIC STUDIES

A typical biomagnetic recording[5] is a superposition of signals produced by the biomagnetic sources, external interference sources, and unidealities of the measurement device. Particular care has to be taken to eliminate the interferences as they are generally several orders of magnitude stronger than the biomagnetic signals and may severely disturb the data analysis and the inherently difficult source modeling task.

Because of the aforementioned problems, several interference reduction or removal methods have been developed. The interferences can be suppressed either by hardware or software methods or by a combination of them. The most common hardware methods include magnetically shielded rooms,[11–13] gradiometer coils,[14] and reference channels.[15] Some of the best-known software methods are based on signal statistics, such as the signal space projection (SSP) combined with the principal component analysis[16] (PCA) and methods based on the independent components analysis (ICA).[17]

All of the compensation methods used to reject the residual interference inside the shielded room suffer from strong and sometimes false assumptions about the magnetic fields. Ideally balanced gradiometer coils provide perfect shielding against homogeneous fields but fail to compensate for more complex fields. The reference channel method assumes that any interference seen by the signal channels can be modeled by a small number of reference channels at a distance from the subject where they are sensitive to the interference only. In contrast, the PCA-based SSP method calculates the dominant interference signals using the signal channels themselves leading to a reliable interference removal method free of distortions caused by inaccurate calibration or geometry information. However, the statistical methods do not perform ideally in situations where the interference patterns differ from the interference subspace predetermined by the statistical analysis. SSS provides a more robust and reliable interference suppression method as compared to the previous methods because it suppresses an arbitrary external interference of magnetic origin with minimal assumptions. With SSS one does not have to know anything about the interference sources or dedicate any channels as reference channels.

Movement-related distortion of the data has traditionally been considered as one of the major inherent limitations of the MEG method. Many subjects, such as small children or some of the patients, may continuously move their head during the measurement. The movement distorts the measured signal and sometimes makes data analysis impossible if no movement compensation is done on the data. Furthermore, even small magnetized particles attached to the head cause large artifacts when moving with respect to the sensors. These artifacts are typical, e.g., for patients with minor impurities left from instruments used in brain surgical operations.

The problem caused by movement can be solved by using the minimum norm estimate[18] as a source model[19] for transforming the measured signals to correspond to a reference head position. The device-independent components of SSS are a similar source model with the benefit of modeling also the external interference signals. Furthermore, the harmonic basis functions of SSS are faster to compute than the lead fields needed with the minimum norm estimate. As a consequence, SSS can be used as an efficient movement-correction method with no distortions caused by external interference.

Also, the magnetized impurities are static objects in the coordinate system of the head and appear as static components in the SSS decomposition. Therefore, the movement artifacts can be eliminated from the movement compensated data by removing the dc component with a simple base line correction thus allowing for examinations of an important patient group so far excluded from MEG.

Measurement of dc or near dc has been difficult with conventional MEG because of the ambiguous response of the SQUID to static fields and because at low frequencies the external interference signals dominate. The physiological dc phenomena can be recorded by movement modulation causing the dc signals to appear as time-varying MEG signals. Previous solutions to measure these signals have included

mechanical modulation[20] by additional instrumentation designed to produce a well-defined movement pattern taken into account in extracting the dc signals. By means of SSS, however, dc measurements can be done as easily as any MEG measurements. The SSS-based dc measurements require the subject to move the head with no predefined frequency or movement pattern. By calculating the device-independent SSS components of the time differences of the signals, one can extract the dc components and, in addition, get rid of the external interferences.

In contrast with most signal space methods, SSS relies on the knowledge about the sensor geometry and calibration coefficients. Reconstruction of the signals is free of bias only if the geometry and calibration are known precisely. In the absence of random noise, any deviation of the measured signal from the SSS-based expansion is caused by our incomplete knowledge about the sensor array. The portion of the deviations caused by uncorrelated sensor noise is normally distributed with zero mean and thus statistically separable from systematic calibration errors. Using SSS, the system can be calibrated to extremely high precision by finding the calibration parameters that minimize the deviations and bring the system to consistency with Maxwell's equations. No probe with precisely known geometry is needed, and the insufficient knowledge on probe geometry does not result in bias of the calibration parameters.

III. HARMONIC BASIS FUNCTIONS FOR SCALAR AND VECTOR FIELDS

The devices used in biomagnetic recordings comprise sensors located in a source-free volume. Furthermore, the quasistatic approximation of Maxwell's equations is justified[5,21] and thus the field recorded by the sensors is a gradient of a harmonic scalar potential,

$$\mathbf{B} = -\mu_0 \nabla V, \tag{1}$$

where μ_0 is the permeability of vacuum and V satisfies Laplace's equation,

$$\nabla^2 V = 0. \tag{2}$$

This potential can be expressed as a linear combination of a complete set of basic solutions of Laplace's equations. For example, with typical multichannel MEG devices it is practical to use spherical coordinates in which case the solution of Laplace's equation can be expanded in spherical harmonics,[22,23]

$$V(\mathbf{r}) = \sum_{l=0}^{\infty}\sum_{m=-l}^{l} \alpha_{lm}\frac{Y_{lm}(\theta,\varphi)}{r^{l+1}} + \sum_{l=0}^{\infty}\sum_{m=-l}^{l} \beta_{lm} r^l Y_{lm}(\theta,\varphi) \equiv V_\alpha(\mathbf{r}) + V_\beta(\mathbf{r}). \tag{3}$$

Throughout this paper, we use complex-valued functions to keep the calculations as compact as possible. However, one could also use, e.g., the real-valued even and odd spherical harmonics[24,25] as the starting point or change from complex to real representation at any point. Here

$$Y_{lm}(\theta,\varphi) = \sqrt{\frac{2l+1}{4\pi}\frac{(l-m)!}{(l+m)!}} P_{lm}(\cos\theta) e^{im\varphi} \tag{4}$$

is the normalized spherical harmonic function, $P_{lm}(\cos\theta)$ is the associated Legendre function, and i denotes imaginary unit. Importantly, expansions $V_\alpha(\mathbf{r})$ and $V_\beta(\mathbf{r})$ correspond separately to source locations $\mathbf{r}'$ with $r'<r$ and $r'>r$, respectively. In this paper, the primed coordinates always refer to the source volume.

The corresponding expansion for the magnetic field $\mathbf{B}(\mathbf{r})$ can be derived using Eqs. (1) and (3). Let us start from the expansion

$$\mathbf{B}(\mathbf{r}) = -\mu_0\sum_{l=0}^{\infty}\sum_{m=-l}^{l} \alpha_{lm}\nabla\left[\frac{Y_{lm}(\theta,\varphi)}{r^{l+1}}\right] - \mu_0\sum_{l=0}^{\infty}\sum_{m=-l}^{l} \beta_{lm}\nabla\left[r^l Y_{lm}(\theta,\varphi)\right]. \tag{5}$$

Application of the gradient operator ∇ gives in spherical coordinates

$$\nabla\left(\frac{Y_{lm}}{r^{l+1}}\right) = \frac{1}{r^{l+2}}\left[-(l+1)Y_{lm}\mathbf{e}_r + \frac{\partial Y_{lm}}{\partial\theta}\mathbf{e}_\theta + \frac{imY_{lm}}{\sin\theta}\mathbf{e}_\varphi\right] \tag{6}$$

and

$$\nabla(r^l Y_{lm}) = r^{l-1}\left(lY_{lm}\mathbf{e}_r + \frac{\partial Y_{lm}}{\partial\theta}\mathbf{e}_\theta + \frac{imY_{lm}}{\sin\theta}\mathbf{e}_\varphi\right), \tag{7}$$

where $\mathbf{e}_r$, $\mathbf{e}_\theta$, and $\mathbf{e}_\varphi$ are the orthogonal unit vectors in the spherical coordinate system and arguments θ and φ have been left out to simplify the expressions. The angular dependence of Eqs. (6) and (7) can be expressed by the modified vector spherical harmonics $\boldsymbol{\nu}_{lm}(\theta,\varphi)$ and $\boldsymbol{\omega}_{lm}(\theta,\varphi)$ (see Appendix A) leading to

$$\mathbf{B}(\mathbf{r}) = -\mu_0\sum_{l=0}^{\infty}\sum_{m=-l}^{l} \alpha_{lm}\frac{\boldsymbol{\nu}_{lm}(\theta,\varphi)}{r^{l+2}} - \mu_0\sum_{l=0}^{\infty}\sum_{m=-l}^{l} \beta_{lm} r^{l-1}\boldsymbol{\omega}_{lm}(\theta,\varphi) \equiv \mathbf{B}_\alpha(\mathbf{r}) + \mathbf{B}_\beta(\mathbf{r}). \tag{8}$$

Thus, the magnetic field, derivable from a harmonic scalar potential, can be expressed as an expansion of orthogonal harmonic vector fields with the same expansion coefficients as in Eq. (3).

Let us now express the multipole moments α_{lm} and β_{lm} with the vector spherical harmonic function $\mathbf{X}_{lm}(\theta,\varphi)$ (see appendix A). The relation between α_{lm} and the underlying current distribution is given by[24,26]

$$\alpha_{lm} = \frac{-1}{(2l+1)(l+1)}\int_{v'} r'^l Y_{lm}^*(\theta',\varphi')\nabla' \cdot[\mathbf{r}'\times\mathbf{J}_{\text{in}}(\mathbf{r}')]dv', \tag{9}$$

where prime refers to source volume, asterisk indicates complex conjugate, and $\mathbf{J}_{\text{in}}(\mathbf{r}')$ is the current distribution in the volume with $r'<r$. Using basic vector identities, the integrand of the above equation can be transformed into form

$\mathbf{r}' \times \nabla'[r'^l Y^*_{lm}(\theta', \varphi')] \cdot \mathbf{J}_{\text{in}}(\mathbf{r}')$. On the other hand, the angular momentum operator encountered in quantum mechanics is given by $\mathbf{L}' = -i(\mathbf{r}' \times \nabla')$ leading to integrand $(1/i)\mathbf{L}'^* r'^l Y^*_{lm}(\theta', \varphi') \cdot \mathbf{J}_{\text{in}}(\mathbf{r}') = (1/i) r'^l \mathbf{L}'^* Y^*_{lm}(\theta', \varphi') \cdot \mathbf{J}_{\text{in}}(\mathbf{r}') = (1/i) r'^l \sqrt{l(l+1)} \mathbf{X}^*_{lm}(\theta', \varphi') \cdot \mathbf{J}_{\text{in}}(\mathbf{r}')$ with the last equality being based on Eq. (A5). Thus, Eq. (9) gets the form

$$\alpha_{lm} = \frac{i}{2l+1} \sqrt{\frac{l}{l+1}} \int_{v'} r'^l \mathbf{X}^*_{lm}(\theta', \varphi') \cdot \mathbf{J}_{\text{in}}(\mathbf{r}') dv'. \quad (10)$$

Consequently, the relation between the current distribution and an individual multipole moment is of the lead field-like presentation,

$$\alpha_{lm} = \int_{v'} \boldsymbol{\lambda}^{\alpha}_{lm}(\mathbf{r}') \cdot \mathbf{J}_{\text{in}}(\mathbf{r}') dv', \quad (11)$$

where, in analogy to the conventional lead fields,

$$\boldsymbol{\lambda}^{\alpha}_{lm}(\mathbf{r}) = \frac{i}{2l+1} \sqrt{\frac{l}{l+1}} r^l \mathbf{X}^*_{lm}(\theta, \varphi). \quad (12)$$

These lead fields are orthogonal over a spherical volume with radius R,

$$\begin{aligned} &\int_v \boldsymbol{\lambda}^{\alpha}_{lm}(\mathbf{r}) \cdot \boldsymbol{\lambda}^{\alpha^*}_{LM}(\mathbf{r}) dv \\ &\quad \propto \int_0^R r^{l+L+2} dr \int_{\Omega} \mathbf{X}^*_{lm}(\theta, \varphi) \cdot \mathbf{X}_{LM}(\theta, \varphi) d\Omega \\ &\quad = \frac{R^{l+L+3}}{l+L+3} \delta_{lL} \delta_{mM}. \end{aligned} \quad (13)$$

Here δ means Dirac's delta function.

The relation between β_{lm} and $\mathbf{J}_{\text{out}}(\mathbf{r}')$ corresponding to the source volume $r' > r$ differs from that of α_{lm} and $\mathbf{J}_{\text{in}}(\mathbf{r}')$ only in the radial part and therefore β_{lm} has the lead field form

$$\beta_{lm} = \int_{v'} \boldsymbol{\lambda}^{\beta}_{lm}(\mathbf{r}') \cdot \mathbf{J}_{\text{out}}(\mathbf{r}') dv', \quad (14)$$

with the lead field

$$\boldsymbol{\lambda}^{\beta}_{lm}(\mathbf{r}) = \frac{i}{2l+1} \sqrt{\frac{l+1}{l}} \frac{\mathbf{X}^*_{lm}(\theta, \varphi)}{r^{l+1}}. \quad (15)$$

Integration similar to Eq. (13) implicates that also the lead fields $\boldsymbol{\lambda}^{\beta}_{lm}(\mathbf{r})$ are orthogonal over a spherical volume. As a conclusion, the multipole moments α_{lm} and β_{lm} are a compact representation of the total current distribution as they contain orthogonal, nonoverlapping information, in contrast with signals of the sensors measuring the magnetic field with nonorthogonal lead fields.

The lead fields $\boldsymbol{\lambda}^{\alpha}_{lm}(\mathbf{r})$ and $\boldsymbol{\lambda}^{\beta}_{lm}(\mathbf{r})$ allow us to expand the total current distribution in an orthogonal basis with angular part $\mathbf{X}^*_{lm}(\theta, \varphi)$. Let us first use a general set $\{\mathbf{j}_{lm}(\mathbf{r})\}$ of orthogonal basis functions in an expansion

$$\mathbf{J}(\mathbf{r}) = \sum_{l=0}^{\infty} \sum_{m=-l}^{l} c_{lm} \mathbf{j}_{lm}(\mathbf{r}), \quad (16)$$

where an individual expansion coefficient is given by

$$c_{lm} = \frac{\int_{v'} \mathbf{j}_{lm}(\mathbf{r}') \cdot \mathbf{J}(\mathbf{r}') dv'}{\int_{v'} \mathbf{j}_{lm}(\mathbf{r}') \cdot \mathbf{j}_{lm}(\mathbf{r}') dv'}, \quad (17)$$

where we can choose $\mathbf{j}_{lm}(\mathbf{r}) = \boldsymbol{\lambda}^{\alpha}_{lm}(\mathbf{r})$. Similar expression using β_{lm} and $\boldsymbol{\lambda}^{\beta}_{lm}(\mathbf{r})$ holds for the external sources and, consequently, the total current distribution can be expanded as

$$\mathbf{J}_{\text{in}}(\mathbf{r}') = \sum_{l=0}^{\infty} \sum_{m=-l}^{l} \alpha_{lm} \eta_{\alpha l} \left(\frac{r'}{R_{\alpha}} \right)^l \mathbf{X}^*_{lm}(\theta', \varphi'), \quad (18)$$

where R_{α} is the radius of the sphere including all sources with $r' < r$ and

$$\eta_{\alpha l} = -i(2l+1)(2l+3) \sqrt{\frac{l+1}{l}} \frac{1}{R_{\alpha}^{l+3}}, \quad (19)$$

and

$$\mathbf{J}_{\text{out}}(\mathbf{r}') = \sum_{l=0}^{\infty} \sum_{m=-l}^{l} \beta_{lm} \eta_{\beta l} \left(\frac{R_{\beta}}{r'} \right)^{l+1} \mathbf{X}^*_{lm}(\theta', \varphi'), \quad (20)$$

where R_{β} is the radius of the sphere excluding all sources with $r' > r$ and

$$\eta_{\beta l} = i(2l+1)(1-2l) \sqrt{\frac{l}{l+1}} R_{\beta}^{l-2}. \quad (21)$$

Note that the estimates for the current distribution are not unique as they are always strictly tangential with respect to the chosen expansion origin. Because of the ambiguity of the magnetic inverse problem, it is impossible to describe all internal degrees of freedom of the source distribution based on the measured multipole moments. One way to characterize the ambiguity is to consider the silent terms of the Taylor expansion of the scalar potential.[25,27]

Finally, by using the orthonormal vector spherical harmonics $\mathbf{V}_{lm} = \boldsymbol{\nu}_{lm} / \sqrt{(l+1)(2l+1)}$ and $\mathbf{W}_{lm} = \boldsymbol{\omega}_{lm} / \sqrt{l(2l+1)}$ and comparing Eqs. (8), (11), (12), (14), and (15), a useful alternative formulation for the magnetic field is found,

$$\begin{aligned} \mathbf{B}(\mathbf{r}) = &-\mu_0 \sum_{l=0}^{\infty} \sum_{m=-l}^{l} f_{lm}(r, R_{\alpha}, \mathbf{J}_{\text{in}}) \mathbf{V}_{lm}(\theta, \varphi) \\ &-\mu_0 \sum_{l=0}^{\infty} \sum_{m=-l}^{l} g_{lm}(r, R_{\beta}, \mathbf{J}_{\text{out}}) \mathbf{W}_{lm}(\theta, \varphi), \end{aligned} \quad (22)$$

where

$$\begin{aligned} f_{lm}(r, R_{\alpha}, \mathbf{J}_{\text{in}}) = &\sqrt{\frac{l}{2l+1}} \int_0^{R_{\alpha}} \int_{\Omega'} \left(\frac{r'}{r} \right)^{l+2} i \mathbf{X}^*_{lm}(\theta', \varphi') \\ &\cdot \mathbf{J}_{\text{in}}(\mathbf{r}') dr' d\Omega' \end{aligned} \quad (23)$$

and

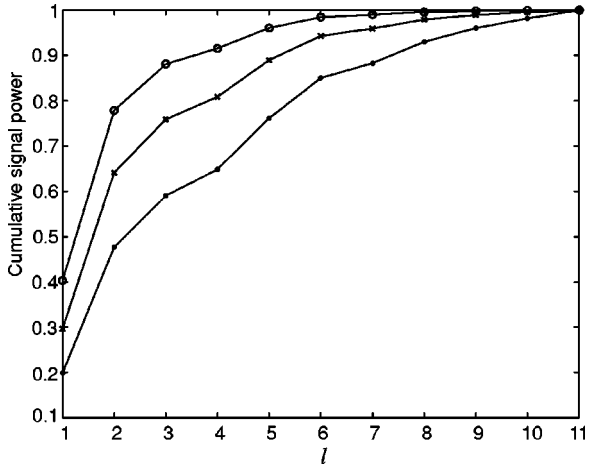

FIG. 1. Cumulative signal power of the internal sources consisting of 100 current dipoles with $r'=7$ cm. The dot corresponds to $r=10$ cm, x corresponds to $r=12$ cm, and circle corresponds to $r=15$ cm.

$$g_{lm}(r,R_\beta,\mathbf{J}_{\text{out}}) = \sqrt{\frac{l+1}{2l+1}}\int_{R_\beta}^{\infty}\int_{\Omega'}\left(\frac{r}{r'}\right)^{l-1} i\mathbf{X}_{lm}^{*}(\theta',\varphi') \cdot \mathbf{J}_{\text{out}}(\mathbf{r}')dr'd\Omega'. \tag{24}$$

Functions $f_{lm}(r,R_\alpha,\mathbf{J}_{\text{in}})$ and $g_{lm}(r,R_\beta,\mathbf{J}_{\text{out}})$ can be used in estimating the error made by truncating the expansion of Eq. (22) because they demonstrate that the individual terms of the expansion decay as $(r'/r)^{l+2}$ for sources with $r'<r$ and as $(r/r')^{l-1}$ for sources with $r'>r$.

As a quantitative demonstration of the significance of functions $f_{lm}(r,R_\alpha,\mathbf{J}_{\text{in}})$ and $g_{lm}(r,R_\beta,\mathbf{J}_{\text{out}})$, Figs. 1 and 2 show the normalized cumulative signal power for two hypothetical source current distributions as a function of l. For each value of l, the signal power corresponding to Eq. (23) is defined as $\sqrt{\Sigma_m f_{lm}^2(r,R_\alpha,\mathbf{J}_{\text{in}})}$ with $m=-l\cdots l$. In Fig. 1, the source consists of 100 current dipoles evenly distributed on a sphere at a distance of 7 cm from the expansion origin in a spherically symmetric conductor model and the signal power has been calculated for three different values of r: 10, 12, and 15 cm. Asymptotic values indicate convergence, and for practical measurements containing noise, truncation with $l \geqslant 8$ is sufficient even for these superficial sources as also supported by experimental data.[10] This can be concluded from the simulations in Ref. 10 showing that truncation-based signal distortions of the order of those in Fig. 2 corresponding to $l \geqslant 8$ are insignificant with practical signal-to-noise ratios of multichannel measurement devices. Similarly, Fig. 2 shows the cumulative signal power corresponding to Eq. (24). In this case, the source consists of 100 dipoles in free space evenly distributed on a spherical surface at a distance of 50 cm from the expansion origin. All other parameters are as in Fig. 1. Clearly, $l \geqslant 3$ suffices for a good representation of these external signals.

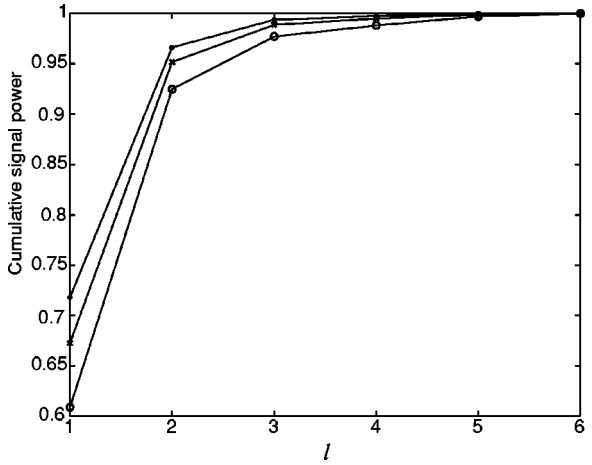

FIG. 2. Cumulative signal power of the external sources consisting of 100 current dipoles with $r'=50$ cm. The dot corresponds to $r=10$ cm, x corresponds to $r=12$ cm, and circle corresponds to $r=15$ cm.

As a practical example, consider the current dipole in a spherically symmetric volume conductor, which is a widely used source model in biomagnetism[5] and defined as a concentration of the primary current to a single point, $\mathbf{J}(\mathbf{r}) = \mathbf{Q}\delta(\mathbf{r}-\mathbf{r}_q)$. In this model, the whole current circuit can be described[28,29] by a triangle having two radial sides and one tangential side in such a way that the radial currents contain the contribution of the volume currents and the tangential component is the primary current $\mathbf{Q}$. From Eq. (11) we immediately see that the contribution of the radial current vanishes provided that the expansion origin equals the origin of the conductor model. Then, by inserting Eq. (11) to Eq. (8), we get

$$\mathbf{B}_{\text{dipole}}(\mathbf{r}) = -\mu_0\sum_{l=0}^{\infty}\frac{1}{2l+1}\sqrt{\frac{l}{l+1}}\sum_{m=-l}^{l} r_q^l i\mathbf{X}_{lm}^{*}(\theta_q,\varphi_q) \cdot \mathbf{Q}\frac{\boldsymbol{\nu}_{lm}(\theta,\varphi)}{r^{l+2}}. \tag{25}$$

This series-form solution, utilizing harmonic functions, provides an alternative for the formula derived by Sarvas.[30]

IV. THE SSS BASIS

A. Harmonic signal space

The geometry of a typical neuromagnetic measurement is illustrated schematically in Fig. 3. Here I_{in} and I_{out} describe the interesting and interference sources, respectively. The harmonic potentials associated with these sources are given in the different volumes by either $V_\alpha(\mathbf{r})$ or $V_\beta(\mathbf{r})$ expansions of Eq. (3) as indicated. Specifically, in volume 3 where the sensor array is located the potential associated with I_{in} is given by the expansion $V_\alpha(\mathbf{r})$, and the potential associated with I_{out} is given by the expansion $V_\beta(\mathbf{r})$. The resolution between the interference and interesting magnetic subspaces in the SSS method is based on this fact.

Let us define the signal vectors $\mathbf{a}_{lm}$ and $\mathbf{b}_{lm}$ as responses of the multichannel measurement device to the individual terms of the expansions $\mathbf{B}_\alpha(\mathbf{r})$ and $\mathbf{B}_\beta(\mathbf{r})$ in Eq. (8). Then any measured signal vector $\boldsymbol{\phi}=[\phi_1\cdots\phi_N]$ corresponding to N channels can be expressed as a linear combination,

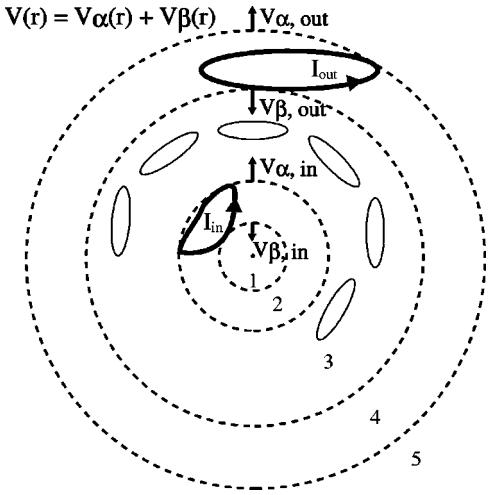

FIG. 3. Geometry of a typical neuromagnetic measurement including the interesting source and an interference source. The origin is in the center. The figure was originally published in Ref. 33.

$$\boldsymbol{\phi} = \sum_{l=1}^{L_{\text{in}}} \sum_{m=-l}^{l} \alpha_{lm}\mathbf{a}_{lm} + \sum_{l=1}^{L_{\text{out}}} \sum_{m=-l}^{l} \beta_{lm}\mathbf{b}_{lm}, \tag{26}$$

provided that L_{in} and L_{out} are large enough. Here we have excluded the components with $l=0$ because they correspond to magnetic monopoles which do not exist according to Maxwell's equation $\nabla\cdot\mathbf{B}=0$.

Equation (26) can be expressed in the compact matrix notation,

$$\boldsymbol{\phi} = \mathbf{S}\mathbf{x} = [\mathbf{S}_{\text{in}}\mathbf{S}_{\text{out}}]\begin{bmatrix}\mathbf{x}_{\text{in}}\\ \mathbf{x}_{\text{out}}\end{bmatrix}, \tag{27}$$

where

$$\mathbf{S}_{\text{in}} = [\mathbf{a}_{1,-1}\ldots\mathbf{a}_{L_{\text{in}}L_{\text{in}}}], \tag{28}$$

$$\mathbf{S}_{\text{out}} = [\mathbf{b}_{1,-1}\ldots\mathbf{b}_{L_{\text{out}}L_{\text{out}}}], \tag{29}$$

$$\mathbf{x}_{\text{in}} = [\alpha_{1,-1}\ldots\alpha_{L_{\text{in}}L_{\text{in}}}]^T, \tag{30}$$

$$\mathbf{x}_{\text{out}} = [\beta_{1,-1}\ldots\beta_{L_{\text{out}}L_{\text{out}}}]^T. \tag{31}$$

Thus, $\mathbf{S}$ is the magnetic subspace, the SSS basis, spanning all measurable magnetic signals, provided that L_{in} and L_{out} are high enough, and it contains separate subspaces $\mathbf{S}_{\text{in}}$ and $\mathbf{S}_{\text{out}}$ spanning the biomagnetic signals and external interference signals, respectively. The corresponding multipole moments are contained in vector $\mathbf{x}$.

It is easy to see from Eq. (26) that the dimension, the number of basis vectors, of the SSS basis is

$$n = (L_{\text{in}}+1)^2 + (L_{\text{out}}+1)^2 - 2. \tag{32}$$

The fundamental requirement for the applicability of SSS is the condition $N>n$. Therefore, it is essential to estimate lower bounds for the orders L_{in} and L_{out} capable of representing any present magnetic field, for example, by using Eqs. (23) and (24).

The SSS basis is linearly independent for practical sensor arrays. In principle, the array has linearly dependent basis vectors only when the sensors are confined into a purely spherical array and all the sensors are either strictly radial or strictly tangential (see Appendix B for a proof). Thus, with a practical sensor array satisfying $N>n$, any measured signal vector can be uniquely decomposed into the multipole moments containing separate amplitudes for the biomagnetic and external interference signals. It is interesting to note that measuring tangential components of the magnetic field enhances the resolution between the biomagnetic and external interference signals.

B. Sensitivity of the SSS basis

This section describes the theoretical relations showing how the SSS reconstruction is affected by random noise and errors in the basis matrix. Practical demonstrations are given in Ref. 10. In the following we assume that noise and magnetic signals are uncorrelated and have zero mean.

1. Noise

The noise sensitivity of the SSS basis depends on the sensor configuration and noise level of the sensors. Let the noise covariance of the device be $\mathbf{N}=\mathbf{E}[\mathbf{n}\mathbf{n}^T]$, where $\mathbf{E}$ means expectation and $\mathbf{n}$ is the signal vector composed of random noise. Furthermore, let the covariance matrix of the expansion amplitudes in Eq. (27) be $\mathbf{C}_x=\mathbf{E}[\mathbf{x}\mathbf{x}^T]$. This covariance is altered by the pseudoinverse $\mathbf{S}^\dagger$ when the amplitudes are estimated from the measured noisy data $\boldsymbol{\phi}=\boldsymbol{\phi}_0+\mathbf{n}$ as the estimate is $\hat{\mathbf{x}}=\mathbf{S}^\dagger\boldsymbol{\phi}=\mathbf{S}^\dagger(\boldsymbol{\phi}_0+\mathbf{n})=\mathbf{x}+\mathbf{S}^\dagger\mathbf{n}$ leading to

$$\mathbf{E}[\hat{\mathbf{x}}\hat{\mathbf{x}}^T] = \mathbf{E}[\mathbf{x}\mathbf{x}^T] + \mathbf{E}[\mathbf{S}^\dagger\mathbf{n}\mathbf{n}^T(\mathbf{S}^\dagger)^T] = \mathbf{C}_x + \mathbf{S}^\dagger\mathbf{N}(\mathbf{S}^\dagger)^T. \tag{33}$$

Thus, the noise increase is characterized by the term $\mathbf{S}^\dagger\mathbf{N}(\mathbf{S}^\dagger)^T$ which combines the sensor geometry through the pseudoinverse of $\mathbf{S}$ and the sensor noise through the noise covariance matrix $\mathbf{N}$.

The SSS-reconstructed internal signal $\hat{\boldsymbol{\phi}}_{\text{in}}$ is also affected by sensor configuration and noise level. Let us define the matrix $\mathbf{P}=[\mathbf{I}\ \mathbf{0}]$, where $\mathbf{I}$ is a $[(L_{\text{in}}+1)^2-1]\times[(L_{\text{in}}+1)^2-1]$-dimensional identity matrix and $\mathbf{0}$ is a $[(L_{\text{in}}+1)^2-1]\times[(L_{\text{out}}+1)^2-1)$-dimensional null matrix. Then $\hat{\mathbf{x}}_{\text{in}}=\mathbf{P}\hat{\mathbf{x}}$ and $\hat{\boldsymbol{\phi}}_{\text{in}}=\mathbf{S}_{\text{in}}\mathbf{P}\hat{\mathbf{x}}$ leading to covariance

$$\mathbf{E}[\hat{\boldsymbol{\phi}}_{\text{in}}\hat{\boldsymbol{\phi}}_{\text{in}}^T] = \mathbf{C}_\phi + \mathbf{S}_{\text{in}}\mathbf{P}\mathbf{S}^\dagger\mathbf{N}(\mathbf{S}^\dagger)^T\mathbf{P}^T\mathbf{S}_{\text{in}}^T, \tag{34}$$

where $\mathbf{C}_\phi=\mathbf{S}_{\text{in}}\mathbf{P}\mathbf{C}_x\mathbf{P}^T\mathbf{S}_{\text{in}}^T$ is the covariance of the signal.

2. Inaccurate knowledge of the sensors

In contrast with sensitivity to random noise, inaccuracies in the knowledge of the sensor geometry and calibration produce systematic bias to the SSS reconstruction. In a way, this is a more severe cause of reconstruction errors than random noise as large systematic bias may significantly affect localization accuracy. Consequently, it is important to estimate the amount of reconstruction bias as a function of geometry and calibration accuracy.

Let us assume a noiseless signal $\boldsymbol{\phi}_0=\mathbf{S}\mathbf{x}$ and define $\tilde{\mathbf{S}}=\mathbf{S}^T\mathbf{S}$ and $\tilde{\boldsymbol{\phi}}_0=\mathbf{S}^T\boldsymbol{\phi}_0$. Then $\tilde{\mathbf{S}}\mathbf{x}=\tilde{\boldsymbol{\phi}}_0$ and the estimated signal based on erroneous amplitude vector $\mathbf{x}+\Delta\mathbf{x}$ and perturbated

matrix $\tilde{\mathbf{S}}+\Delta\tilde{\mathbf{S}}$ is $\tilde{\boldsymbol{\phi}}=(\tilde{\mathbf{S}}+\Delta\tilde{\mathbf{S}})(\mathbf{x}+\Delta\mathbf{x})$, where the perturbation of the matrix is caused by geometry and calibration inaccuracies. The estimation error depends on the condition number $\kappa(\tilde{\mathbf{S}})$ of matrix $\tilde{\mathbf{S}}$ and the matrix error,[31]

$$\frac{\|\Delta\mathbf{x}\|}{\|\mathbf{x}+\Delta\mathbf{x}\|} \leqslant \kappa(\tilde{\mathbf{S}})\frac{\|\Delta\tilde{\mathbf{S}}\|}{\|\tilde{\mathbf{S}}\|}. \tag{35}$$

On the other hand, the estimation error of the signal vector $\hat{\boldsymbol{\phi}}=(\mathbf{S}+\Delta\mathbf{S})(\mathbf{x}+\Delta\mathbf{x})$ satisfies

$$\begin{aligned}\|\hat{\boldsymbol{\phi}}-\boldsymbol{\phi}_0\| &\leqslant \|\mathbf{S}\|\|\Delta\mathbf{x}\|+\|\Delta\mathbf{S}\|\|\mathbf{x}+\Delta\mathbf{x}\| \\ &\leqslant \left[\|\Delta\mathbf{S}\|+\kappa(\tilde{\mathbf{S}})\frac{\|\Delta\tilde{\mathbf{S}}\|}{\|\tilde{\mathbf{S}}\|}\|\mathbf{S}\|\right]\|\mathbf{x}+\Delta\mathbf{x}\|. \end{aligned}\tag{36}$$

This worst case estimate is generally too pessimistic in practice, as shown by extensive demonstrations,[10] but it shows that the reconstruction error is proportional both to the matrix error and the condition number of the unperturbated matrix. Therefore, the condition number of the SSS basis should be kept as low as possible by proper design of the sensor array.[32]

V. APPLICATIONS OF SSS

A. Suppression of external interferences

The separation of the SSS basis into the biomagnetic subspace $\mathbf{S}_{\text{in}}$ and the external interference subspace $\mathbf{S}_{\text{out}}$ in Eq. (27) allows one to remove the interferences by reconstructing the signals using only components of the biomagnetic subspace. First, an estimate $\hat{\mathbf{x}}$ for the multipole moments is calculated from the measured signal vector $\boldsymbol{\phi}$ by modeling both the biomagnetic and external interference signals,

$$\hat{\mathbf{x}}=\begin{bmatrix}\hat{\mathbf{x}}_{\text{in}}\\ \hat{\mathbf{x}}_{\text{out}}\end{bmatrix}=\mathbf{S}^{\dagger}\boldsymbol{\phi}, \tag{37}$$

where $\mathbf{S}^{\dagger}=(\mathbf{S}^T\mathbf{S})^{-1}\mathbf{S}^T$ is the pseudoinverse of $\mathbf{S}$ or a regularized version of this inversion. Then the biomagnetic signals can be reconstructed from the estimate leaving out the contribution of the external interferences,

$$\hat{\boldsymbol{\phi}}_{\text{in}}=\mathbf{S}_{\text{in}}\hat{\mathbf{x}}_{\text{in}}. \tag{38}$$

As a consequence, all signals arising from volumes 4 and 5 of Fig. 3 are eliminated in the reconstruction. Practical examples of the external interference suppression have been shown in Refs. 33 and 10.

B. Virtual signals and movement correction

The vector of multipole moments $\mathbf{x}$ is device-independent enabling biomagnetic signals to be transformed between sensor arrays. Thus, transformation of the biomagnetic signals from a measurement device with SSS basis $\mathbf{S}$ to a virtual device with SSS basis $\mathbf{S}_v$ is done simply by

$$\hat{\boldsymbol{\phi}}_v=\mathbf{S}_{v,\text{in}}\hat{\mathbf{x}}_{\text{in}}, \tag{39}$$

where $\hat{\mathbf{x}}_{\text{in}}$ has been estimated from the measurement according to Eq. (37).

The virtual signal calculation generalizes to a movement-correction method as one can transform the measured signals from a moving subject to a virtual sensor array locked to the subject's head, provided that a continuous head movement monitoring method is available.[19]

The simplest way to perform a movement-corrected evoked measurement is to average the device-independent multipole moments instead of the traditional way of averaging the data epochs. After the measurement, one can calculate by Eq. (39) the virtual signals corresponding to a desired reference head position by using the averaged multipole moments.

However, a much faster movement-correction method avoiding consecutive pseudoinverses is achieved by noting that the head movements and magnetic fields are independent random variables. Consequently, the averaged signal $\langle\boldsymbol{\phi}\rangle$ is of the form

$$\langle\boldsymbol{\phi}\rangle=\langle\mathbf{S}\mathbf{x}\rangle=\langle\mathbf{S}\rangle\langle\mathbf{x}\rangle, \tag{40}$$

where the second equality comes from independence. Thus, the movement correction can be done using the averaged data $\langle\boldsymbol{\phi}\rangle$ and averaged SSS basis $\langle\mathbf{S}\rangle$ in Eq. (37) and the resulting $\langle\hat{\mathbf{x}}\rangle_{\text{in}}$ in Eq. (39). The average of the SSS basis $\langle\mathbf{S}\rangle$ corresponds to averaging the bases of different head positions during the measured data epochs.

In the case of large movements, the signal-to-noise ratio (SNR) may vary significantly between different epochs corresponding to different positions of the subject. Therefore, it may be necessary to calculate the weighted averages

$$\langle\mathbf{S}\rangle=\frac{1}{w_s}\sum_{i=1}^{M}w_i\mathbf{S}_i \tag{41}$$

and

$$\langle\boldsymbol{\phi}\rangle=\frac{1}{w_s}\sum_{i=1}^{M}w_i\boldsymbol{\phi}_i, \tag{42}$$

where M is the number of epochs and $w_s=\Sigma_i w_i$. A suitable weighting factor can be derived from the theoretical upper bound of the SNR corresponding to the position of the object during the ith epoch,

$$\text{SNR}=\frac{\|\boldsymbol{\phi}_{\text{in},i}\|}{\|\mathbf{n}\|}=\frac{\|\mathbf{S}_{\text{in},i}\mathbf{x}_{\text{in}}\|}{\|\mathbf{n}\|}\leqslant\|\mathbf{S}_{\text{in},i}\|\frac{\|\mathbf{x}_{\text{in}}\|}{\|\mathbf{n}\|}, \tag{43}$$

where $\mathbf{n}$ is a noise signal and $\|\cdot\|$ indicates some suitable norm. Thus, the upper bound of SNR is proportional to $\|\mathbf{S}_{\text{in},i}\|$ and we can choose

$$w_i=\|\mathbf{S}_{\text{in},i}\|. \tag{44}$$

C. dc measurements

Static sources, the dc, can be measured by SQUID sensors only if the dc sources move with respect to the sensors as the SQUIDs are sensitive to dynamic signals only. Thus,

in order to measure the dc of the human brain the subject has to move with respect to the sensor array. One way to accomplish this is to move a bed sinusoidally back and forth while the subject is lying on the bed in a fixed position.[20]

As an alternative and easier method, the movement-correction method described in Sec. V B enables one to monitor the dc signals. As the multipole moments $\mathbf{x}_{\text{in}}$ corresponding to the biomagnetic sources are calculated in the head coordinate system, the static magnetic fields of the brain, measurable only from a moving subject, can be extracted. Consequently, voluntary head movements can be used for detection of dc phenomena of the brain. On the other hand, the undesirable movement artifacts caused by magnetic impurities can be removed by removing the dc component after movement correction, e.g., by doing base line correction.[34] A specifically powerful method to extract the dc component can be formulated by considering the signal differences as described in Ref. 35.

VI. DISCUSSION

SSS is a method to remove external disturbances, to calculate virtual signals, to perform movement correction, and to measure signals caused by dc. SSS also facilitates source modeling by representing the measured magnetic signals as components containing orthogonal information about the underlying current distribution.

The ability of SSS to span practically all MEG signals is based on the fact that the number of channels in modern multichannel devices clearly exceeds the number of degrees of freedom of the measurable magnetic fields produced by the brain and interference sources. Thus, it is possible to decompose in a stable manner any measured signal into the basis components by exploiting the oversampling condition.

In this paper we have shown that in quasistatic approximation, the magnetic field can be expressed by an expansion of vector spherical harmonics. By using these harmonic functions, SSS models both the interesting and disturbance signals uniquely forming a very robust disturbance removal method. Reconstruction of the interesting signals using only the corresponding multipole moments with disturbances removed is in principle arbitrarily accurate if the calibration and geometry of the measurement device are precisely known.

The multipole moments are device independent which immediately enables a straightforward way to perform movement correction and calculate virtual signals to any desired sensor configuration. Furthermore, the device independency also enables dc measurements with SQUIDs and facilitates removal of movement artifacts caused by static magnetic objects.

The multipole moments can be expressed as projections of the current distribution to their lead fields. Because these lead fields are orthogonal, the multipole moments are a compact representation of the measured data. Furthermore, the lead fields have a simple mathematical form encouraging one to use the multipole moments for source modeling despite the lack of obvious physiological correlations between the multipoles and MEG sources beyond the dipole. This is a topic of future research.

As a conclusion, SSS greatly improves the quality of biomagnetic data without requiring essential user intervention, e.g., in the form of user selectable-free parameters, a particularly important feature in clinical MEG work.

ACKNOWLEDGMENTS

The authors would like to thank Dr. Juha Simola for fruitful discussions about the SSS method and support in the method development. We also wish to acknowledge Dr. Antti Ahonen, Dr. Jukka Nenonen, Dr. John Mosher, and Dr. Matti Hämälainen for comments and criticism on the manuscript.

APPENDIX A: VECTOR SPHERICAL HARMONICS

Arfken[22] and Hill[36] define the following vector spherical harmonic functions:

$$\mathbf{V}_{lm}(\theta,\varphi) = \frac{1}{\sqrt{(l+1)(2l+1)}}\left[-(l+1)Y_{lm}(\theta,\varphi)\mathbf{e}_r + \frac{\partial Y_{lm}(\theta,\varphi)}{\partial\theta}\mathbf{e}_\theta + \frac{imY_{lm}(\theta,\varphi)}{\sin\theta}\mathbf{e}_\varphi\right], \tag{A1}$$

$$\mathbf{W}_{lm}(\theta,\varphi) = \frac{1}{\sqrt{l(2l+1)}}\left[lY_{lm}(\theta,\varphi)\mathbf{e}_r + \frac{\partial Y_{lm}(\theta,\varphi)}{\partial\theta}\mathbf{e}_\theta + \frac{imY_{lm}(\theta,\varphi)}{\sin\theta}\mathbf{e}_\varphi\right], \tag{A2}$$

$$\mathbf{X}_{lm}(\theta,\varphi) = \frac{-1}{\sqrt{l(l+1)}}\left[\frac{mY_{lm}(\theta,\varphi)}{\sin\theta}\mathbf{e}_\theta + i\frac{\partial Y_{lm}(\theta,\varphi)}{\partial\theta}\mathbf{e}_\varphi\right] \tag{A3}$$

satisfying the orthonormality condition,

$$\int_\Omega \mathbf{P}_{lm}(\theta,\varphi)\cdot\mathbf{R}^*_{LM}(\theta,\varphi)d\Omega = \delta_{PR}\delta_{lL}\delta_{mM}, \tag{A4}$$

where Ω is the solid angle and $\mathbf{P}$ and $\mathbf{R}$ may be $\mathbf{V}$, $\mathbf{X}$ or $\mathbf{W}$.

Function $\mathbf{X}_{lm}(\theta,\varphi)$ can also be expressed using the normalized scalar spherical harmonic function $Y_{lm}(\theta,\varphi)$,[22,23]

$$\mathbf{X}_{lm}(\theta,\varphi) = \frac{1}{\sqrt{l(l+1)}}\mathbf{L}Y_{lm}(\theta,\varphi), \tag{A5}$$

where $\mathbf{L}$ is the angular momentum operator,

$$\mathbf{L} = -i(\mathbf{r}\times\nabla). \tag{A6}$$

Let us also define the modified vector spherical functions,

$$\boldsymbol{\nu}_{lm}(\theta,\varphi) = \sqrt{(l+1)(2l+1)}\mathbf{V}_{lm}(\theta,\varphi) \tag{A7}$$

and

$$\boldsymbol{\omega}_{lm}(\theta,\varphi) = \sqrt{l(2l+1)}\mathbf{W}_{lm}(\theta,\varphi), \tag{A8}$$

which are orthogonal over solid angle according to Eqs. (A1), (A2), and (A4).

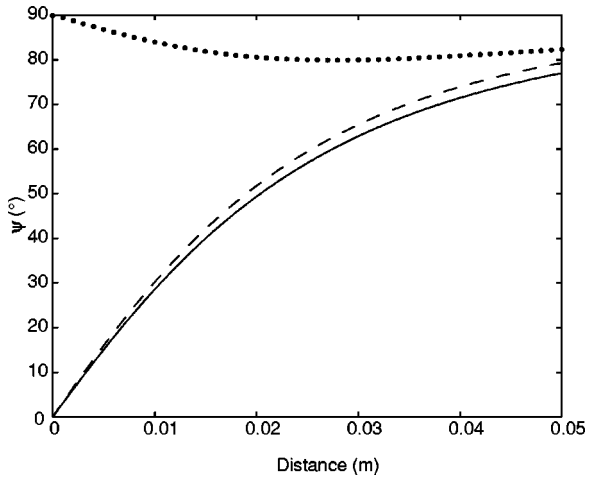

FIG. 4. The largest principal angle as a function of distance between the two spheres containing sensors. Solid curve: all sensors radial, dashed curve: all sensors tangential, and dotted curve: both radial and tangential sensors.

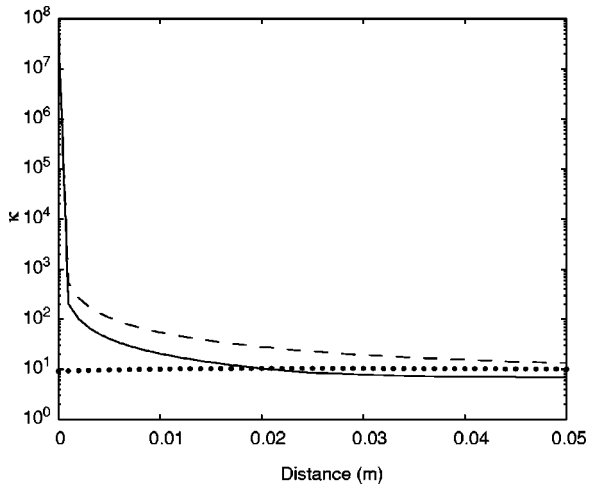

FIG. 5. Condition number of normalized **S** as a function of distance between the two spheres containing sensors. Solid curve: all sensors radial, dashed curve: all sensors tangential, and dotted curve: both radial and tangential sensors.

APPENDIX B: LINEAR INDEPENDENCE OF THE SSS BASIS

According to elementary linear algebra, the columns of the SSS basis **S** are linearly independent only if

$$\boldsymbol{\phi} = \mathbf{S}\mathbf{x} = \mathbf{0} \Rightarrow \mathbf{x} = \mathbf{0} \Leftrightarrow \alpha_{lm} = \beta_{lm} = 0 \;\forall\; l,m. \tag{B1}$$

Without loss of generality, suppose the sensors are pointlike magnetometers, $L_{\text{in}}=L_{\text{out}}=L$, and that the number of sensors satisfies $N>2(L+1)^2-2$. Furthermore, we assume that the sensors are confined to two distinct surfaces separated by a finite distance. If this distance is zero, the sensors are located on a single surface.

According to Eq. (8), the output of the jth sensor having location $\mathbf{r}_j$ and normal vector $\mathbf{n}_j=n_{jr}\mathbf{e}_r+n_{j\theta}\mathbf{e}_\theta+n_{j\varphi}\mathbf{e}_\varphi$ is then

$$\phi_j = -\mu_0 \sum_{l,m} \left\{ \left[-(l+1)\frac{\alpha_{lm}}{r_j^{l+2}} + l\beta_{lm} r_j^{l-1} \right] n_{jr} Y_{lm} + \left(\frac{\alpha_{lm}}{r_j^{l+2}} + \beta_{lm} r_j^{l-1} \right) \left(n_{j\theta} \frac{\partial Y_{lm}}{\partial \theta} + n_{j\varphi} \frac{imY_{lm}}{\sin\theta_j} \right) \right\}, \tag{B2}$$

where the argument of Y_{lm} has been left out for simplicity. We note that

$$-\sqrt{l(l+1)}i\mathbf{e}_r \times \mathbf{X}_{lm} = \frac{\partial Y_{lm}}{\partial \theta}\mathbf{e}_\theta + \frac{imY_{lm}}{\sin\theta}\mathbf{e}_\varphi \tag{B3}$$

and from Hill's equations[36] we get

$$-\sqrt{l(l+1)}i\mathbf{e}_r \times \mathbf{X}_{lm} = \sqrt{\frac{l(l+1)}{2l+1}}\left[\sqrt{l}\mathbf{V}_{lm} + \sqrt{l+1}\mathbf{W}_{lm}\right] \tag{B4}$$

and

$$Y_{lm}\mathbf{e}_r = \frac{1}{\sqrt{2l+1}}\left[-\sqrt{l+1}\mathbf{V}_{lm} + \sqrt{l}\mathbf{W}_{lm}\right]. \tag{B5}$$

According to the orthogonality relations of the vector spherical harmonics, functions $Y_{lm}\mathbf{e}_r$ and $\sqrt{l(l+1)}i\mathbf{e}_r\times\mathbf{X}_{lm}$ form a set of orthogonal functions over a spherical volume, with the property that any linear combination of such functions can be zero only when each function is multiplied by zero. Combination of Eqs. (B2) and (B3) gives

$$\phi_j = -\mu_0 \sum_{l,m} \left\{ \left[-(l+1)\frac{\alpha_{lm}}{r_j^{l+2}} + l\beta_{lm} r_j^{l-1} \right] Y_{lm}\mathbf{e}_r \cdot \mathbf{n}_j - \left(\frac{\alpha_{lm}}{r_j^{l+2}} + \beta_{lm} r_j^{l-1} \right) \sqrt{l(l+1)}i\mathbf{e}_r \times \mathbf{X}_{lm} \cdot \mathbf{n}_j \right\} \tag{B6}$$

The second term of the sum vanishes for radial sensors ($\mathbf{n}_j=n_{jr}\mathbf{e}_r$) and similarly the first term of the sum vanishes for tangential sensors ($\mathbf{n}_j=n_{j\theta}\mathbf{e}_\theta+n_{j\varphi}\mathbf{e}_\varphi$). Due to the orthogonality condition, in the radial case the solution of $\phi_j=0$ from Eq. (B6) is

$$\alpha_{lm} = \frac{l}{l+1}\beta_{lm} r_j^{2l+1} \;\forall\; l,m \tag{B7}$$

and similarly the solution of $\phi_j=0$ in the tangential case is

$$\alpha_{lm} = -\beta_{lm} r_j^{2l+1} \;\forall\; l,m. \tag{B8}$$

In order for a nontrivial solution to exist for $\boldsymbol{\phi}=\mathbf{S}\mathbf{x}=\mathbf{0}$, Eqs. (B7) and (B8) have to be valid on each channel indicating that $r_j=r_0\,\forall\, j$ with r_0 being arbitrary. Furthermore, Eqs. (B7) and (B8) do not have a common solution apart from the trivial one, meaning that each channel has to be radial or each channel has to be tangential. This also means that in the general case with $\mathbf{n}_j=n_{jr}\mathbf{e}_r+n_{j\theta}\mathbf{e}_\theta+n_{j\varphi}\mathbf{e}_\varphi$ the only solution for $\boldsymbol{\phi}=\mathbf{S}\mathbf{x}=\mathbf{0}$ is the trivial solution $\alpha_{lm}=\beta_{lm}=0\,\forall\, l,m$. As a conclusion, the SSS basis is linearly dependent for a spherical array with strictly radial or strictly tangential sensors.

To examine the linear independence quantitatively, we simulated the effect of the non-sphericality of the sensor array on the SSS basis with $L_{\text{in}}=L_{\text{out}}=6$. In the simulation, the condition number κ of **S** and the largest principal angle ψ between $\mathbf{S}_{\text{in}}$ and $\mathbf{S}_{\text{out}}$ were calculated for an array consisting of 397 pointlike magnetometers. The distance between two equidimensional subspaces is defined as $\sin\psi$ with ψ being the largest principal angle between the subspaces.[37]

In the first simulation the sensors were equally distributed on two spherical surfaces and Fig. 4 shows the principal angle as a function of distance between the surfaces. With the zero distance all sensors are located on the same sphere and $\psi=0$ for an array consisting of radial or tangential sensors. In these cases $\mathbf{S}_{\text{in}}$ and $\mathbf{S}_{\text{out}}$ become linearly dependent. However, an array consisting of both radial and tangential sensors has $\psi>0$ even when the sensors are located on the same spherical surface. With nonzero distance between the two spheres, ψ is nonzero also for the radial and tangential sensors. These observations are in accordance with the mathematical proof shown above. A further confirmation is given by Fig. 5 showing the condition number of the normalized SSS basis using the same paradigm as in Fig. 4. The condition number is practically infinite for the radial and tangential sensors when the sensors are located on the same sphere. In other cases κ is finite indicating linear independence.

[1]J. P. Wikswo, Phys. Today **57**, 15 (2004).
[2]J. Clarke and A. Barginski, *The SQUID Handbook* (Wiley-VCH, Weinham, 2004).
[3]M. Pannetier, C. Fermon, G. L. Goff, J. Simola, and E. Kerr, Science **304**, 1648 (2004).
[4]I. Kominis, T. Kornack, J. Allred, and M. Romalis, Nature (London) **422**, 596 (2003).
[5]M. Hamalainen, R. Hari, R. J. Ilmoniemi, J. Knuutila, and O. V. Lounasmaa, Rev. Mod. Phys. **65**, 413 (1993).
[6]J. Nenonen, M. Kajola, J. Simola, and A. Ahonen, *Proceedings of the 14th International Conference on Biomagnetism*, edited by E. Halgren, S. Ahlfors, M. Hamalainen, and D. Cohen (Biomag2004 Ltd., Boston, MA, 2004), pp. 630–631.
[7]A. Ahonen, M. Hamalainen, R. Ilmoniemi, M. Kajola, J. Knuutila, J. Simola, and V. Vilkman, IEEE Trans. Biomed. Eng. **40**, 859 (1993).
[8]J. Malmivuo, *Acta Polytechnica Scandinavica*, Electrical Engineering Series No. 39 (The Finnish Academy of Technical Sciences, Helsinki, 1976).
[9]J. Tripp, *Biomagnetism: An Interdisclipinary Approach*, edited by S. J. Williamson, G.-L. Romani, L. Kaufman, and I. Modena (Plenum, New York, 1983), pp. 101–139.
[10]S. Taulu, J. Simola, and M. Kajola, IEEE Trans. Signal Process. (in press).
[11]D. Cohen, Rev. Phys. Appl. **5**, 53 (1970).
[12]V. Kelha, J. Pukki, R. Peltonen, A. Penttinen, R. Ilmoniemi, and J. Heino, IEEE Trans. Magn. **MAG-18**, 260 (1982).
[13]J. Bork, H.-D. Hahlbohm, R. Klein, and A. Schnabel, *Proceedings of the 12th International Conference on Biomagnetism*, edited by J. Nenonen, R. J. Ilmoniemi, and T. Katila (Helsinki University of Technology, Espoo, Finland, 2001), pp. 970–973.
[14]J. E. Zimmerman, J. Appl. Phys. **48**, 702 (1977).
[15]J. Vrba and S. E. Robinson, Methods **25**, 249 (2001).
[16]M. Uusitalo and R. Ilmoniemi, Med. Biol. Eng. Comput. **35**, 135 (1997).
[17]R. Vigário, J. Sarela, V. Jousmaki, M. Hamalainen, and E. Oja, IEEE Trans. Biomed. Eng. **47**, 589 (2000).
[18]M. Hamalainen and R. Ilmoniemi, Med. Biol. Eng. Comput. **32**, 35 (1994).
[19]K. Uutela, S. Taulu, and M. Hamalainen, Neuroimage **14**, 1424 (2001).
[20]B.-M. Mackert, G. Wuebbeler, M. Burghoff, P. Marx, L. Trahms, and G. Curio, Neurosci. Lett. **273**, 159 (1999).
[21]R. Plonsey and D. Heppner, Bull. Math. Biophys. **29**, 657 (1967).
[22]G. Arfken, *Mathematical Methods for Physicists* (Academic Press, Orlando, 1985).
[23]J. D. Jackson, *Classical Electrodynamics* (John Wiley & Sons, Inc., New York, 1999).
[24]K. Jerbi, J. Mosher, S. Baillet, and R. Leahy, Phys. Med. Biol. **47**, 523 (2002).
[25]J. P. Wikswo, J. Appl. Phys. **56**, 3039 (1984).
[26]J. Bronzan, Am. J. Phys. **39**, 1357 (1971).
[27]J. P. Wikswo, J. Appl. Phys. **57**, 4301 (1985).
[28]R. Ilmoniemi, Ph.D. thesis, 1985.
[29]R. Ilmoniemi, M. Hamalainen, and J. Knuutila, *Biomagnetism: Applications & Theory*, edited by H. Weinberg, G. Stroink, and T. Katila (Pergamon Press, New York, 1985), pp. 278–282.
[30]J. Sarvas, Phys. Med. Biol. **32**, 11 (1987).
[31]E. Kreyszig, *Advanced Engineering Mathematics* (John Wiley & Sons, Inc., New York, 1993).
[32]S. Taulu, J. Simola, M. Kajola, and J. Nenonen, *Proceedings of the 14th International Conference on Biomagnetism*, edited by E. Halgren, S. Ahlfors, M. Hamalainen, and D. Cohen (Biomag2004 Ltd., Boston, MA, 2004), pp. 186–187.
[33]S. Taulu, M. Kajola, and J. Simola, Brain Topogr **16**, 269 (2004).
[34]Patent application FI20040070 (pending).
[35]S. Taulu, J. Simola, and M. Kajola, *Proceedings of the 14th International Conference on Biomagnetism*, edited by E. Halgren, S. Ahlfors, M. Hamalainen, and D. Cohen (Biomag2004 Ltd., Boston, MA, 2004), pp. 184–185.
[36]E. L. Hill, Am. J. Phys. **22**, 211 (1954).
[37]G. H. Golub and C. F. Van Loan, *Matrix Computations* (The Johns Hopkins University Press, Baltimore, MD, 1996).